ADVANCED FUNCTIONAL MATERIALS
www.afm-journal.de

High Performance $Mg_2(Si,Sn)$ Solid Solutions: a Point Defect Chemistry Approach to Enhancing Thermoelectric Properties

Guangyu Jiang, Jian He, Tiejun Zhu, Chenguang Fu, Xiaohua Liu, Lipeng Hu, and Xinbing Zhao**

A point defect chemistry approach to improving thermoelectric (TE) properties is introduced, and its effectiveness in the emerging mid-temperature TE material $Mg_2(Si,Sn)$ is demonstrated. The TE properties of $Mg_2(Si,Sn)$ are enhanced via the synergistical implementation of three types of point defects, that is, Sb dopants, Mg vacancies, and Mg interstitials in $Mg_2Si_{0.4}Sn_{0.6-x}Sb_x$ with high Sb content ($x > 0.1$), and it is found that i) Sb doping at low ratios tunes the carrier concentration while it facilitates the formation of Mg vacancies at high doping ratios ($x > 0.1$). Mg vacancies act as acceptors and phonon scatters; ii) the concentration of Mg vacancies is effectively controlled by the Sb doping ratio; iii) excess Mg facilitates the formation of Mg interstitials that also tunes the carrier concentration; vi) at the optimal Sb-doping ratio near $x \approx 0.10$ the lattice thermal conductivity is significantly reduced, and a state-of-the-art figure of merit ZT > 1.1 is attained at 750 K in 2 at% Zn doped $Mg_2Si_{0.4}Sn_{0.5}Sb_{0.1}$ specimen. These results demonstrate the significance of point defects in thermoelectrics, and the promise of point defect chemistry as a new approach in optimizing TE properties.

1. Introduction

The impending energy crisis and environmental issues associated with the use of fossil fuel have imposed a pressing demand for sustainable energy conversion technologies, including thermoelectricity. Thermoelectric (TE) devices can directly inter-convert heat and electricity.[1,2] The conversion efficiency largely depends on the figure of merit of the material, $ZT = \alpha^2\sigma T/\kappa$, where α is the Seebeck coefficient, σ the electrical conductivity, κ the thermal conductivity (including the lattice thermal conductivity κ_L and the electronic thermal conductivity κ_e), and T the absolute temperature. Among the ZT-governing physical properties, the power factor ($PF = \alpha^2\sigma$) and the lattice thermal conductivity κ_L are relatively less interdependent, leading to two basic strategies to improving ZT. One is to enhance the PF by tuning the carrier concentration, [2] or increasing the effective mass via band convergence[3–5] and resonant levels.[6,7] The other is to reduce κ_L via enhancing phonon scattering in solid solutions and/or at the grain boundaries,[7,8] for example, in PbTe(PbSe),[9] Bi_2Te_3[10,11] and filled skutterudites.[12] In the same spirit, the material parameter $\beta = (m^*/m_e)^{3/2}\mu/\kappa_L$ has been used as a criterion for high-ZT materials,[13] where m^* is the carrier effective mass, and μ the carrier mobility in $cm^2\ V\ s^{-1}$ and κ_L in $W\ cm^{-1}\ K^{-1}$.

Notably, Mg_2X (X = Si, Ge, and Sn)-based materials exhibit large β values,[14] promising mid-temperature TE performance,[3,15,16] and also they are made of non-toxic and naturally abundant constituent elements. To date, the best TE performance with ZT~1 has been attained in $Mg_2(Si,Sn)$ solid solutions, in line with enhancing the PF (i.e., the first strategy) via implementing low carrier scattering potential,[17] band convergence,[18] and group-VA elements doping.[3,15] However, the experimentally minimum κ_L of $Mg_2(Si,Sn)$ ($\approx$1.5 $W\ m^{-1}\ K^{-1}$) is substantially higher than the state-of-the-art TE materials, such as Bi_2Te_3 (<1.0 $W\ m^{-1}\ K^{-1}$) [10] and PbTe ($\approx$1.0 $Wm^{-1}K^{-1}$).[4] Hence the promise of $Mg_2(Si,Sn)$-based materials as an emerging class of green mid-temperature TE materials hinges on how to further reduce the lattice thermal conductivity without degrading the PF much.

The optimal operation temperature range of $Mg_2(Si,Sn)$ is in the mid-temperature range, where the characteristic wavelength of heating-carrying phonons, λ, is on the order of its lattice constant, a, according to the relation $\lambda \approx (\theta_D/T)\ a$, where θ_D is

G. Y. Jiang, Prof. T. J. Zhu, C. G. Fu, X. H. Liu, L. P. Hu, Prof. X. B. Zhao
State Key Laboratory of Silicon Materials
Department of Materials Science and Engineering
Zhejiang University, Hangzhou 310027
People's Republic of China
E-mail: zhutj@zju.edu.cn; zhaoxb@zju.edu.cn
G. Y. Jiang, Prof. T. J. Zhu, C. G. Fu, Prof. X. B. Zhao
Key Laboratory of Advanced Materials and Applications for Batteries of Zhejiang Province
Zhejiang University
Hangzhou 310027, People's Republic of China
Dr. J. He
Department of Physics and Astronomy
Clemson University
Clemson, SC, 29634–0978, USA

DOI: 10.1002/adfm.201400123

the Debye temperature.[19] When the characteristic length scale of phonon scatters is comparable to λ or a, the phonons can be more strongly scattered. In view of the simple antifluorite crystal structure of $Mg_2(Si,Sn)$, implementation of point defects is the option.

There are basically three types of point defects in $Mg_2(Si,Sn)$, that is, dopants, vacancies and interstitials. Kato et al. studied the point defects in Mg_2Si by density functional theory and proposed that donor-like Mg interstitials are the major point defects in both Mg-rich and Mg-poor conditions.[20] Experimentally, Liu et al. and Du et al. confirmed that Mg interstitials act as donors and effectively increase the carrier concentration and TE properties of $Mg_2(Si,Sn)$.[21,22] A small amount of Sb dopants (<3%) at Si/Sn sites as donors also contribute electrons to $Mg_2(Si,Sn)$.[16,17,23] Nolas et al. and Dasgupta et al. systematically studied the roles of Mg vacancy in $Mg_2(Si,Sb)$. They found that a high Sb doping ratio (≈10%) facilitates the formation of Mg vacancies; Mg vacancies act as acceptors and thus compensate for the Sb doping; Mg vacancies strongly scatter phonons but they adversely affect the carrier concentration and the carrier mobility.

An immediate question arises as to whether the three types of point defects, Si/Sn-site dopants, Mg vacancies, and Mg interstitials can be synergistically implemented in $Mg_2(Si,Sn)$ to further optimize its TE performance. To address this question, one needs a feasible experimental control of each type of defect to study the interplay between Si/Sn-site dopants, Mg vacancies, and Mg interstitials. First, we note that Sb doping on Si/Sn sites effectively adjusts the carrier concentration and the concentration of Mg vacancies. At low doping ratios (<3%), Sb doping increases the electron concentration ($Sb \rightarrow Sb_{Sn}^{\cdot} + e'$).[3,18,21,22] However, at higher doping ratios (≈10% in Mg_2Si)[23] Sb doping facilitates the formation of Mg vacancies ($Sb \rightarrow Sb_{Sn}^{\cdot} + \frac{1}{2}V''_{Mg}$) to conserve charge neutrality.[24] In the simplest case (without Mg interstitials), charge neutrality leads to a relation $[V''_{Mg}] = \frac{1}{2}[Sb_{Sn}^{\cdot}]$, where $[V''_{Mg}]$ and $[Sb_{Sn}^{\cdot}]$ are the concentration of Mg vacancies and the Sb-doping ratio, respectively. We will experimentally verify this relation in the following. Second, Mg interstitials can be formed and controlled by excess Mg in the starting material.[17,22] However, one concern is that vacancies and interstitials are thermodynamically meta-stable and tend to recombine (similar to Frenkel defects), leading to hysteretic behavior in TE properties. In a supplemental study (Figure S1, Supporting Information), we have conducted electrical conductivity, Seebeck coefficient on the specimens containing both Mg vacancies and Mg interstitials up to 750 K for multiple times. We found no noticeable changes: the recombination process, if any, is negligible under current experimental conditions. It is plausible to infer that the Sb dopants stabilize Mg vacancies and inhibit the recombination process. Accordingly we can independently control the concentration of Mg interstitial in the presence of Sb-dopants and Mg vacancies. Finally, we note that Mg vacancies act as acceptors while Sb-dopants and Mg interstitials act as donors, their interplay adds another layer of control of the carrier concentration. In this work, we will investigate the interplay of Sb doping, Mg vacancies and Mg interstitials in $Mg_2(Si,Sn)$ solid solutions, and demonstrate the point defect chemistry approach can be effective in enhancing TE properties.

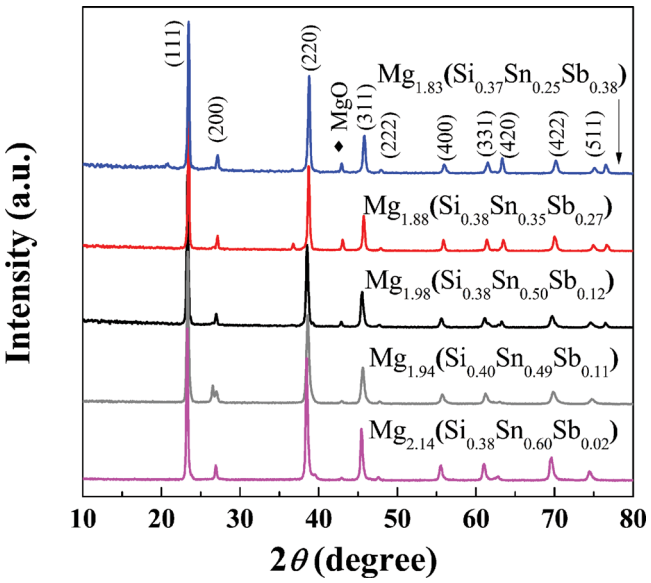

Figure 1. XRD patterns of all $Mg_2Si_{0.4}Sn_{0.6-x}Sb_x$ specimens. The actual compositions are determined by EPMA. Solid diamond (♦) denotes the MgO impurity phase.

2. Results and Discussion

Figure 1 presents the XRD patterns of all $Mg_2Si_{0.4}Sn_{0.6-x}Sb_x$ specimens with the actual Sb compositions $x = 0.02, 0.11, 0.12, 0.27, 0.38$ (EPMA compositions, hereafter). All major reflections can be well indexed to the antifluorite structure (space group $Fm\bar{3}m$), suggesting that the solid solubility limit of Sb in $Mg_2(Si,Sn)$ is higher than $x = 0.38$, similar to Nolas's results.[23] A trace amount of MgO was observed in all specimens but it won't alter the following discussion or conclusions. **Table 1** lists the actual composition determined by EPMA along with room temperature physical properties for each specimen. Apparently, Mg deficiency increases with increasing Sb doping ratio, consistent with the formation of more Mg vacancies at higher Sb-doping ratios. On the other hand, the carrier concentration doesn't show any clear trend with either Mg content or Sb content, which is attributed to the interplay between Sb dopants (donors), Mg vacancies (acceptors) and Mg interstitials (donors).

Figure 2a presents the temperature dependence of electrical conductivity σ. We note that σ does not show any clear trend in its magnitude or temperature dependence with the Sb content, similar to the n. The $x = 0.02$ and $x = 0.12$ specimens exhibit

Table 1. Actual compositions and room temperature values of several physical parameters of all $Mg_2Si_{0.4}Sn_{0.6-x}Sb_x$ specimens.

Nominal composition	EPMA composition	n [10^{19} cm^{-3}]	μ [cm^2 V^{-1} s^{-1}]	m^*/m_e
$x = 0.02$	$Mg_{2.14}(Si_{0.38}Sn_{0.60}Sb_{0.02})$	22	57	1.66
$x = 0.10$ (0.5%Mg excess)	$Mg_{1.94}(Si_{0.40}Sn_{0.49}Sb_{0.11})$	0.81	92	1.60
$x = 0.10$	$Mg_{1.98}(Si_{0.38}Sn_{0.50}Sb_{0.12})$	37	38	2.35
$x = 0.25$	$Mg_{1.88}(Si_{0.38}Sn_{0.35}Sb_{0.27})$	18	31	1.35
$x = 0.35$	$Mg_{1.83}(Si_{0.37}Sn_{0.25}Sb_{0.38})$	11	23	1.19

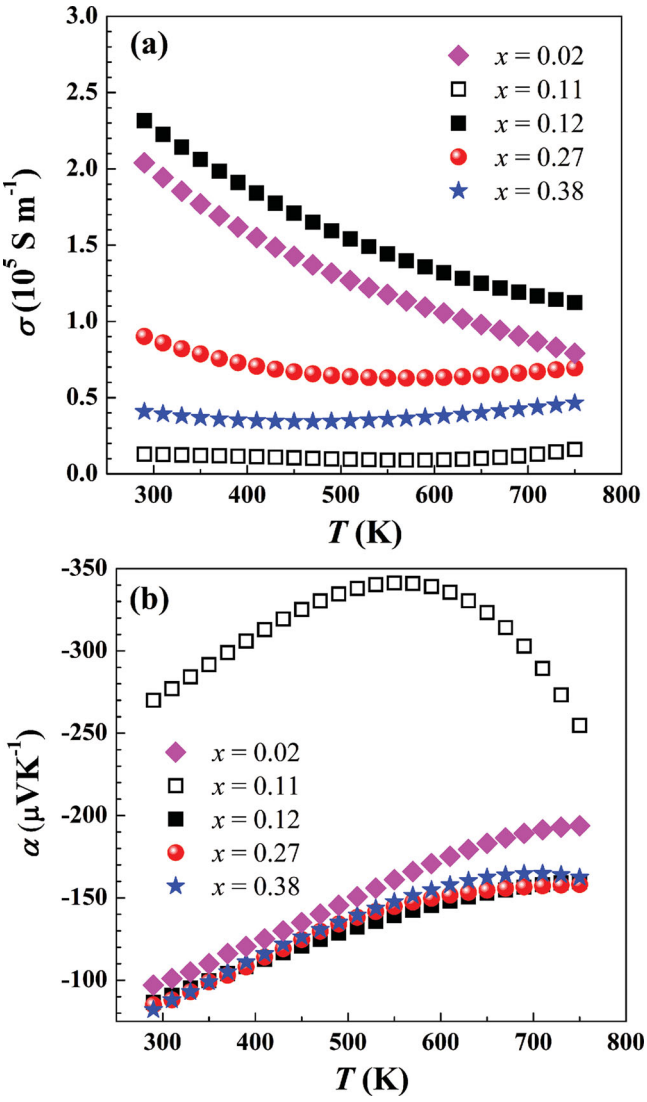

Figure 2. a) Temperature dependence of electrical conductivity σ and b) temperature dependence of the Seebeck coefficient α for $Mg_2Si_{0.4}Sn_{0.6-x}Sb_x$ (x = 0.02, 0.11, 0.12, 0.27, 0.38).

typical temperature dependence of degenerate semiconductors and the highest σ value among all specimens. Notably, the x = 0.11 specimen exhibits a room temperature σ value of about one order of magnitude lower than the x = 0.02 and x = 0.12 specimens along with a very weak temperature dependence. The σ of x = 0.27 and x = 0.38 specimens are somewhat in between in both magnitude and temperature dependence.

The non-systematic variation of σ sheds insight on the interplay between the Sb-dopants, Mg vacancies and Mg interstitials. We first compare x = 0.11 and 0.12 specimens that have same nominal Sb content, slightly different Mg content but distinct σ. Note that the carrier concentration n of x = 0.12 specimen is ≈ 45 times as much as that of x = 0.11 specimen (Table 1), in addition, the α of x = 0.11 specimen exhibits a higher magnitude than all other specimens along with a marked bipolar peak near 550 K (Figure 2b). The bipolar peak signatures a two-band conduction, accordingly the measured R_H and thus n largely reflect the mobility-weighted difference between the electron concentration, n_e, and the hole concentration, n_h,

$$R_H = \frac{n_h\mu_h^2 - n_e\mu_e^2}{e(n_h\mu_h + n_e\mu_e)} \quad (1)$$

where μ_e, μ_h are the electron and hole mobility, respectively. In view of Equation 1, the low n value in x = 0.11 specimen points to a near cancellation between electrons (contributed by Sb-dopants and Mg interstitials) and holes (contributed by Mg vacancies). That is why a few percent difference in Mg content between x = 0.11 and x = 0.12 specimens can cause an order of magnitude change in the n (Table 1). Now we bring x = 0.02 specimen into comparison. In x = 0.02 specimen, Mg interstitials account for the Mg excess and thus most carriers ($Mg \rightarrow Mg_i^{\cdot\cdot} + 2e'$), which is consistent with the previous results.[21,22] Furthermore, it is inferred that the electrons have higher mobility than the holes in $Mg_2(Si,Sn)$, the electrical properties are thus governed more by donors (Sb-dopants and My interstitials) than acceptors (Mg vacancies).

Nonetheless, the role of Mg vacancies becomes more prominent as $x \geq 0.11$, resulting in the reduction in electron concentration and electrical conductivity. Here we try to estimate the concentration of Mg vacanciesfor those specimens with $x \geq 0.11$. Mg vacancy originates from two parts: one is the Mg loss due to the evaporation, the other is the formation of Mg interstitials. The analysis is based on a relation, $[V''_{Mg}] = y + [Mg_i^{\cdot\cdot}]$, where $[Mg_i^{\cdot\cdot}]$ and y represent the concentration of Mg interstitials, and the Mg deficiency per unit volume, respectively. As discussed above, the electron and hole concentrations are nearly cancelled out in the x = 0.11 specimen, so the variation of n at $x \geq 0.11$ is subject to the competition between $[Mg_i^{\cdot\cdot}]$ (donors) and $[V''_{Mg}]$ (acceptors). The contribution of Sb dopant to the carrier concentration is cancelled by the formation of Mg vacancy to conserve charge neutrality. If we assume Mg interstitials account for all carrier concentration, that is, the concentration of Mg interstitial is half of the n as $Mg \rightarrow Mg_i^{\cdot\cdot} + 2e'$, we can estimate $[V''_{Mg}]$ via the relation $[V''_{Mg}] = y + [Mg_i^{\cdot\cdot}] = y + n/2$ for specimens x = 0.11, 0.12, 0.27 and 0.38, with the y values derived from EPMA determined Mg deficiency per unit cell and the n values by Hall coefficient measurements. The Mg vacancy concentrations of all the specimens are listed in **Table 2**. **Figure 3** presents the estimated number of Mg vacancies per molecular formula versus the Sb-content per molecular formula, along with the results previously reported in $Mg_2(Si,Sb)$ by Nolas et al.[23] The data points clearly fall on a straight line with a slope ≈ 1/2, indicating one Mg vacancy is created by nearly two Sb dopants

Table 2. Calculated scattering parameters due to total mass fluctuation Γ_m, Mg-vacancy mass fluctuation $\Gamma_{m,vacancy}$, and strain field scattering Γ_s. Γ_{exp} are the experimentally obtained scattering parameter.

Sb content	$[V''_{Mg}]$ (cal.)	Γ_m (10^3)	$\Gamma_{m,vacancy}$ (10^3)	Γ_s (10^3)	Γ_{exp} (10^3)
0.02	–	–	–	–	–
0.11	0.06	6.3	6.1	13	19
0.12	0.07	7.3	6.9	13	20
0.27	0.14	14	14	15	29
0.38	0.19	18	18	18	36

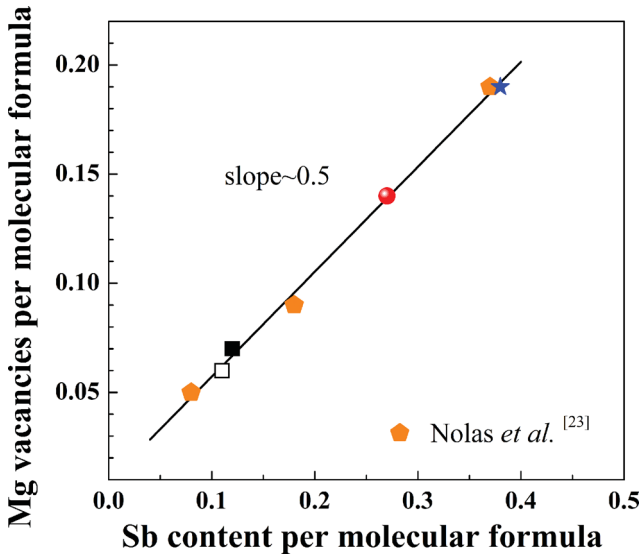

Figure 3. Calculated Mg vacancies per molecular formula as a function of Sb content per molecular formula. We have converted the units of carrier concentration n from cm^{-3} to per molecular formula accordingly. The open circles are experimental data, while the hollow asterisks are calculated from the data reported elsewhere.[23]

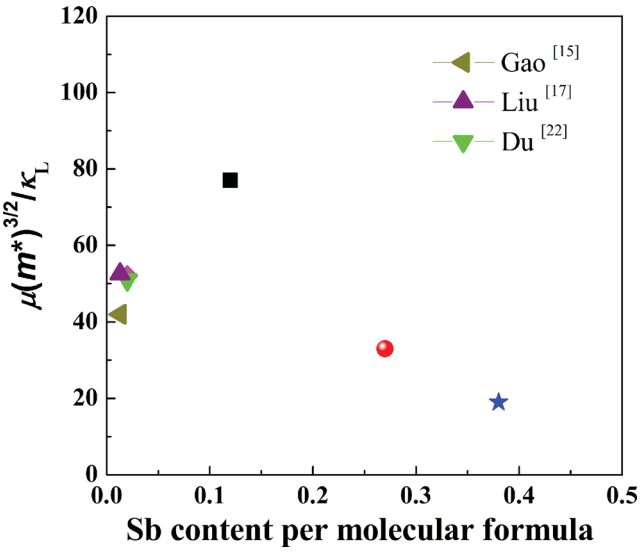

Figure 4. Room temperature value of $(m^*/m_e)^{3/2}\mu/\kappa_L$ as a function of Sb content per molecular formula, m*, μ, and κ_L are discussed in detail in the main text. The lattice thermal conductivities κ_L will be presented in Figure 5b.

in the presence of Mg interstitials and agreeing well with the argument $[V''_{Mg}]=\frac{1}{2}[Sb^{\cdot}_{Sn}]$ we made earlier. The slope is slightly lower than 1/2, which can be attributed to the secondary contribution of Mg vacancies as acceptors. Despite several simplifying assumptions in the analysis, the observed correlation $[Sb^{\cdot}_{Sn}]$ between and $[V''_{Mg}]$ can serve as a guideline for further optimizing $Mg_2(Si,Sn)$-based TE materials via point defect chemistry approach.

Figure 2b shows that the Seebeck coefficient α of all specimens is negative in the temperature range studied, indicative of n-type conduction despite the presence of Mg vacancies (acceptors). The magnitude and temperature dependence of α for all specimens are typical of degenerate semiconductor. Interestingly, except for $x = 0.11$ specimen, all other specimens exhibit very similar α in magnitude and temperature dependence despite a wide variance in their n and σ (Table 1). The significance of this observation will be addressed in conjunction with the band structure parameters next.

To gain more insight on the interplay of these point defects and the impact on the electrical transport properties, we apply a single parabolic band (SPB) model to calculate the electron effective mass m^*.[25] We take the scattering parameter of $r = -1/2$ for a mixed scattering of acoustic phonons and alloy disorder scattering.[17] The values of μ and m^* at room temperature are presented in Table 1. Roughly, both μ and m^* first increase and then decrease with increasing Sb content. The turning point is near $x = 0.11$ and $x = 0.12$ specimens. As discussed above, the material parameter $\beta = (m^*/m_e)^{3/2}\mu/\kappa_L$ is used to gauge the TE potential of a material. **Figure 4** shows the room temperature value of β as a function of Sb content per molecular formula, along with the data points from previous reports for comparison.[15,22] The β value appears to peak somewhere near $x = 0.10$, suggesting that Mg interstitials are thermoelectrically favored whereas Mg vacancies are less favored. The region near $x = 0.10$ is of special interest. It is where Mg vacancies start to form and compensate for the Sb doping, and thus where the impact of Mg interstitials can be maximized.

Figure 5a,b show the temperature dependences of κ and κ_L, respectively. Lattice thermal conductivity, κ_L, is estimated by $\kappa = \kappa_L + \kappa_e$, where $\kappa_e = \sigma L_0 T$ is the electron thermal conductivity. The Lorenz number L_0 can be calculated by SPB model.[21,22] As shown in Figure 5b, the κ_L of all the specimens systematically decreases with increasing Sb content. Especially, the κ_L are almost the same below 570 K for the two specimens ($x = 0.11$ and 0.12) that have a similar Sb content but different $[Mg^{\cdot\cdot}_i]$. As the heat-carrying phonons have a wavelength on the order of the lattice constant, the reduction of κ_L can be explained in term of alloying scattering. Alloy scattering results from the mass fluctuation and strain field fluctuation between the host and impurity atoms. The scattering parameter Γ_{exp} is calculated to describe the total fluctuation in a material (more details in Supporting Information), $\Gamma_{exp} = \Gamma_m + \Gamma_s$,[26] where Γ_m and Γ_s are scattering parameters due to mass fluctuation and strain field scattering, respectively. We present the results of Γ_{exp}, Γ_m, and Γ_s for all the specimens in Table 2. We are fully aware the risk of over-interpreting these numbers from fitting, thus we restrict ourselves to discussing the trend.

The Γ_{exp} in Table 2 shows that alloy scattering is systematically enhanced with increasing Sb content. At low Sb doping ratios, Γ_m is smaller than Γ_s, indicating a predominant strain-field-fluctuation scattering. As the Sb content increases, Γ_m systematically increases until it is about equal to Γ_s. Note that the mass-fluctuation scattering has two contributors, the mass difference between Sn/Sb and that between Mg/Mg vacancies. As shown in Table 2, $\Gamma_{m,vacancy} \approx \Gamma_m$ for all specimens, indicating the phonon scattering due to the mass difference between Mg and Mg vacancy predominates over that between Sb and Sn. Meanwhile, Γ_s also systematically increases with increasing Sb content, indicating that the strain-field scattering is enhanced with Sb doping.

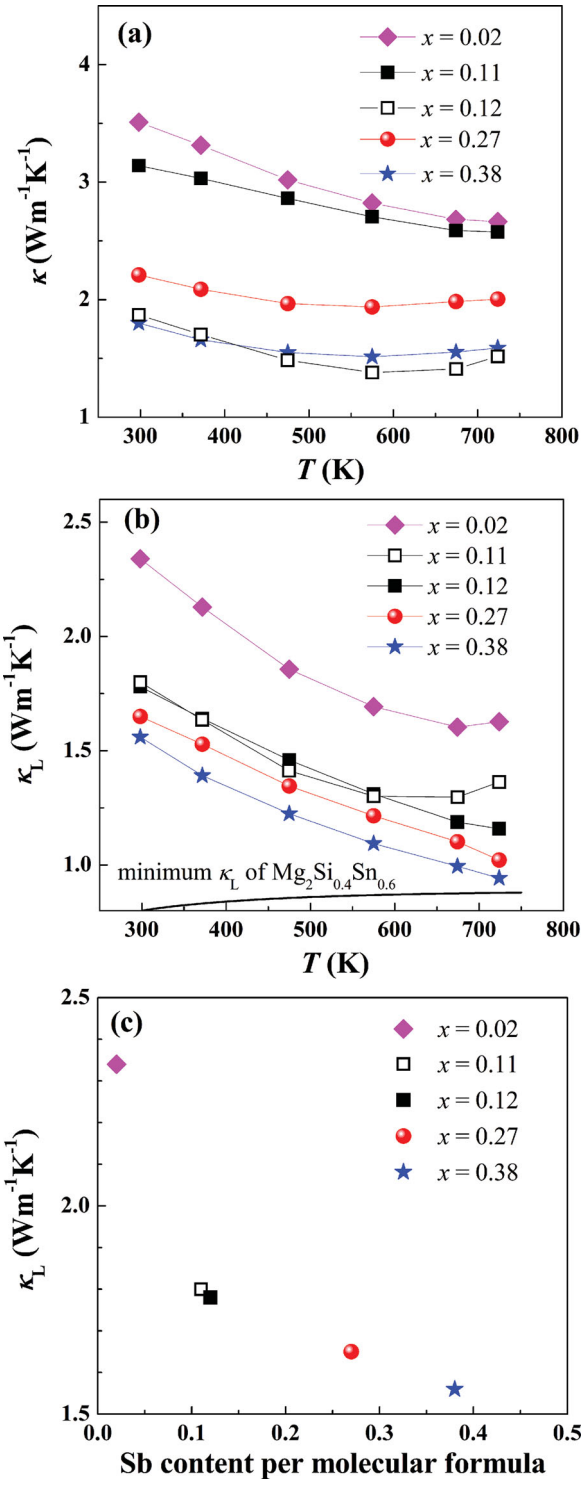

Figure 5. Temperature dependences of a) thermal conductivity κ and b) lattice thermal conductivity κ_L for $Mg_2Si_{0.4}Sn_{0.6-x}Sb_x$ (x = 0.02, 0.11, 0.12, 0.27, 0.38). c) The room temperature κ_L as a function of Sb content per molecule formula.

The strain-field-fluctuation is mainly due to Mg vacancies and partially to the radius difference between Sb and Sn.

We plot the room temperature κ_L versus Sb content per molecular formula in Figure 5c, the results are similar to what

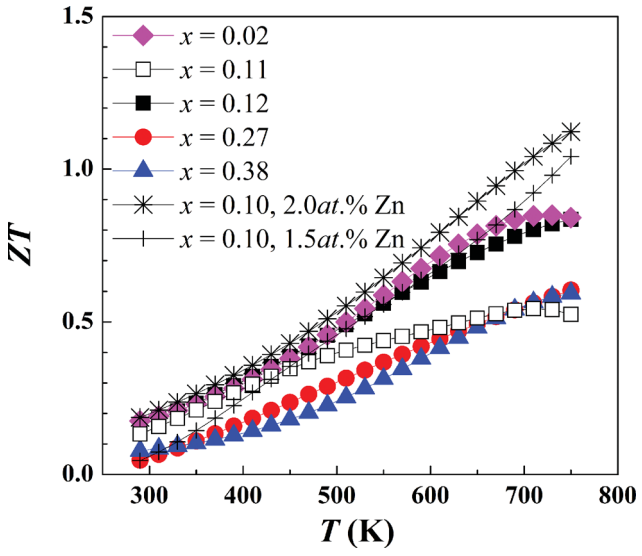

Figure 6. Temperature dependence of ZT for $Mg_2Si_{0.4}Sn_{0.6-x}Sb_x$ (x = 0.02, 0.11, 0.12, 0.27, 0.38) specimens.

Nolas et al. reported in $Mg_2(Si,Sb)$.[23] The large Sb substitution ($x > 0.11$), along with the resulting Mg vacancies, results in a significant reductionof κ_L (>15% near room temperature) compared to that of the x = 0.02 specimen. The κ_L of the x = 0.38 specimen is comparable to the theoretical minimum κ_L, estimated using the Cahill model (Figure 5b).[27] These results thus demonstrated the effectiveness of point defect approach in suppressing the κ_L.

With all TE properties known, we calculate and plot the figure of merit, ZT, of all specimens in **Figure 6**. Importantly, the interplay between Sb-dopants, Mg vacancies and Mg interstitials helps retain the electrical properties over a range of x or n (Figures 4, 6). In particular, the region near $x \sim 0.10$ is of special interest with significantly reduced lattice thermal conductivity and subject to further optimization. However, further optimizing electrical properties of this composition by changing Mg excess and Sb content will destroy the balance between the Sb dopants, Mg vacancies and Mg interstitials. Thus, in a supplemental study, we further tune the n by doping Zn. Indeed, the PF is effectively enhanced and a state-of-the-art $ZT \approx 1.1$ at ≈750 K has been attained for $Mg_2Si_{0.4}Sn_{0.5}Sb_{0.1}$ at 2at% Zn doping (Figure 6).

3. Conclusions

We adopted a point defect chemistry approach to enhancing the TE performance of $Mg_2(Si,Sn)$ via synergistically implementing Sb-dopants on Si/Sn sites, Mg vacancies and Mg interstitials. Among specimens with actual composition $Mg_2Si_{0.4}Sn_{0.6-x}Sb_x$ (x = 0.02, 0.11, 0.12, 0.27, 0.38), we found i) a strong correlation between the Sb content and the concentration of Mg vacancy in the presence of Mg interstitials, which can serve a guideline for further optimization of $Mg_2(Si,Sn)$ based materials; and ii) the interplay between Sb-dopants, Mg vacancies, and Mg interstitials renders a special region near $x \approx 0.10$ in which the TE properties are somewhat decoupled. A state-of-the-art $ZT \approx 1.1$ was attained in $Mg_2Si_{0.4}Sn_{0.50}Sb_{0.10}$ at 750 K upon 2% Zn

doping. These results thus demonstrated the promise of point defect chemistry approach in further optimizing $Mg_2(Si,Sn)$-based TE materials.

4. Experimental Section

$Mg_2Si_{0.4}Sn_{0.6-x}Sb_x$ specimens with nominal composition x = 0.02, 0.10, 0.10, 0.25, 0.30 were prepared. Stoichiometric amount of Mg (3N), Si(3N), Sn (3N), and Sb(5N) powders were weighed and mixed, with 6 at% Mg excess to compensate for the evaporation loss in all specimens except for one specimen (x = 0.10) in which only 0.5at% Mg excess was applied to study the roles of Mg interstitials. The admixture was sealed in a tantalum tube in Ar atmosphere and heated at 1073 K for10 h. The product was pulverized and sieved. Fine powder of size < 75 μm was then hot pressed at 973K for 2h into ϕ 12.6 mm diameter pellets. All pellets have a similar packing density > 95%.

The phase purity of specimens was checked on a Rigaku D/MAX02550PC diffractometer with monochromatic Cu Kα radiation. The chemical compositions were characterized by electron probe microanalysis (EPMA, JEOL-JXA-8100)with a wavelength dispersive spectrometer (WDS).Thermal diffusivity D and specific heat C_p measurements were performed on a Netzsch LFA457 Micro Flash Analyzer. The thermal conductivity was calculated by the relation $\kappa = d\ D\ C_p$, where d is the density of specimen. Then bar specimens were cut from the pellets for electrical conductivity (σ) and Seebeck coefficient (α) measurements on a custom designed apparatus using a DC four-probe method and differential voltage/temperature technique, respectively.[22] The compounds adopt a cubic crystal structure in the temperature range studied, so the TE properties are isotropic. All TE properties, σ, α, and κ, were measured from room temperature to 723 K. The room temperature Hall coefficient (R_H) was measured at 300 K using a Mini Cryogen Free Measurement Systems. The carrier concentration (n) and the carrier mobility (μ) were then estimated by the relation $n = 1/e\ R_H$ and $\mu = R_H\sigma$, where e is the elemental charge. The analysis of defect chemistry is in the context of an ionic picture if not otherwise noted.

Supporting Information

Supporting Information is available from the Wiley Online Library or from the author.

Acknowledgements

The work was supported by the National Basic Research Program of China (2013CB632503), the National Natural Science Foundation of China (51061120455 and 51271165), the Program for Innovative Research Team in University of Ministry of Education of China (IRT13037), the Program for New Century Excellent Talents in University (NCET-12–0495), and the National Science Foundation of the United States (DMR-1008073 and DMR 1307740).

Received: January 14, 2014
Revised: February 10, 2014
Published online: April 1, 2014

[1] T. M. Tritt, *Science* **1999**, *283*, 804.
[2] G. J. Snyder, E. S. Toberer, *Nat. Mater.* **2008**, *7*, 105.
[3] H. Wang, Z. M. Gibbs, Y. Takagiwacand, G. J. Snyder, *Energy Environ. Sci.* **2014**, *7*, 804.
[4] Y. Z. Pei, X. Y. Shi, A. LaLonde, H. Wang, L. D. Chen, G. J. Snyder, *Nature* **2011**, *473*, 66.
[5] H. Wang, Aaron D. LaLonde , Y. Z. Pei, G. J. Snyder, *Adv. Funct. Mater.* **2013**, *23*, 1586.
[6] J. P. Heremans, B. Wiendlocha, A. M. Chamoire, *Energy Environ. Sci* **2012**, *5*, 5510.
[7] C. M. Jaworski, B. Wiendlocha, V. Jovovic, J. P. Heremans, *Energy Environ. Sci* **2011**, *4*, 4155.
[8] C. Yu, T.-J. Zhu, R.-Z. Shi, Y. Zhang, X.-B. Zhao, J. He, *Acta Mater.* **2009**, *57*, 2757.
[9] L. D. Zhao, S. Q. Hao, S. H. Lo, C. I. Wu, X. Y. Zhou, Y. Lee, H. Li, K. Biswas, T. P. Hogan, C. Uher, C. Wolverton, V. P. Dravid, M. G. Kanatzidis, *J. Am. Chem. Soc.* **2013**, *135*, 7364.
[10] L. Hu, H. Gao, X. Liu, H. Xie, J. Shen, T. Zhu, X. Zhao, *J. Mater. Chem.* **2012**, *22*, 16484.
[11] L. P. Hu, X. H. Liu, H. H. Xie, J. J. Shen, T. J. Zhu, X. B. Zhao, *Acta Mater.* **2012**, *60*, 4431.
[12] X. Shi, J. Yang, J. R. Salvador, M. Chi, J. Y. Cho, H. Wang, S. Bai, J. Yang, W. Zhang, L. Chen, *J. Am. Chem. Soc.* **2011**, *133*, 7837.
[13] (Ed: C. B. Vining), *CRC Handbook of Thermoelectrics*, CRC Press, Boca Raton, FL **1995**.
[14] J. Tani, H. Kido, *J. Alloy. Compd.* **2008**, *466*, 335.
[15] H. Gao, T. Zhu, X. Liu, L. Chen, X. Zhao, *J. Mater. Chem.* **2011**, *21*, 5933.
[16] Q. Zhang, H. Yin, X. B. Zhao, J. He, X. H. Ji, T. J. Zhu, T. M. Tritt, *Phys. Status Solidi A* **2008**, *205*, 1657.
[17] X. Liu, T. Zhu, H. Wang, L. Hu, H. Xie, G. Jiang, G. J. Snyder, X. Zhao, *Adv. Energy Mater.* **2013**, *3*, 1238.
[18] W. Liu, X. Tan, K. Yin, H. Liu, X. Tang, J. Shi, Q. Zhang, C. Uher, *Phys. Rev. Lett.* **2012**, *108*, 166601.
[19] (Ed: H. M. Rosenberg), *The Solid State*, Oxford University Press, Oxford **1988**.
[20] A. Kato, T. Yagi, N. Fukusako, *J. Phys. Condens. Matter.* **2009**, *21*, 205801.
[21] W. Liu, X. F. Tang, H. Li, J. Sharp, X. Y. Zhou, C. Uher, *Chem. Mat.* **2011**, *23*, 5256.
[22] Z. Du, T. Zhu, Y. Chen, J. He, H. Gao, G. Jiang, T. M. Tritt, X. Zhao, *J. Mater. Chem.* **2012**, *22*, 6838.
[23] G. S. Nolas, D. Wang, M. Beekman, *Phys. Rev. B.* **2007**, *76*, 235204.
[24] J. S. Cook, J. S. Dryden, *J. Phys. Condens. Matter.* **1981**, *14*, 1133.
[25] G. A. Slack, M. A. Hussain, *J. Appl. Phys.* **1991**, *70*, 2694.
[26] (Ed: T. M. Tritt), *Thermal Conductivity: Theory, Properties, and Applications*, Kluwer Academic, New York, USA **2004**.
[27] D. G. Cahill, S. K. Watson, R. O. Pohl, *Phys. Rev. B* **1992**, *46*, 6131.